doi:10.1016/j.jmb.2008.01.078 J. Mol. Biol. (2008) 378, 941–951

JMB

Available online at www.sciencedirect.com

ScienceDirect

ELSEVIER

A Large Collapsed-state RNA Can Exhibit Simple Exponential Single-molecule Dynamics

Glenna J. Smith[1,4], Kang Taek Lee[1,4], Xiaohui Qu[2,4], Zheng Xie[1,4], Jelena Pesic[1,4], Tobin R. Sosnick[3,4], Tao Pan[3] and Norbert F. Scherer[1,4]*

[1]*Department of Chemistry, University of Chicago, Chicago, Illinois 60637, USA*

[2]*Department of Physics, University of Chicago, Chicago, Illinois 60637, USA*

[3]*Department of Biochemistry and Molecular Biology, University of Chicago, Chicago, Illinois 60637, USA*

[4]*Institute for Biophysical Dynamics, University of Chicago, Chicago, Illinois 60637, USA*

Received 8 December 2007; received in revised form 22 January 2008; accepted 23 January 2008
Available online 4 February 2008

The process of large RNA folding is believed to proceed from many collapsed structures to a unique functional structure requiring precise organization of nucleotides. The diversity of possible structures and stabilities of large RNAs could result in non-exponential folding kinetics (e.g. stretched exponential) under conditions where the molecules have not achieved their native state. We describe a single-molecule fluorescence resonance energy transfer (FRET) study of the collapsed-state region of the free energy landscape of the catalytic domain of RNase P RNA from *Bacillus stearothermophilus* (C_{thermo}). Ensemble measurements have shown that this 260 residue RNA folds cooperatively to its native state at ≥1 mM Mg^{2+}, but little is known about the conformational dynamics at lower ionic strength. Our measurements of equilibrium conformational fluctuations reveal simple exponential kinetics that reflect a small number of discrete states instead of the expected inhomogeneous dynamics. The distribution of discrete dwell times, collected from an "ensemble" of 300 single molecules at each of a series of Mg^{2+} concentrations, fit well to a double exponential, which indicates that the RNA conformational changes can be described as a four-state system. This finding is somewhat unexpected under [Mg^{2+}] conditions in which this RNA does not achieve its native state. Observation of discrete well-defined conformations in this large RNA that are stable on the seconds timescale at low [Mg^{2+}] (<0.1 mM) suggests that even at low ionic strength, with a tremendous number of possible (weak) interactions, a few critical interactions may produce deep energy wells that allow for rapid averaging of motions within each well, and yield kinetics that are relatively simple.

Edited by D. E. Draper

Keywords: FRET; single molecule; RNA folding; collapsed state

Introduction

RNA folding is structurally hierarchical due to three effects: the stacking of bases facilitated by base-pair hydrogen bonding, the electrostatic screening of the polyanionic backbone by mono-or divalent cations, and specific binding of cations.[1,2] Sequestering base pairs in local runs of helical secondary structure occurs very early (i.e., at low ionic strength) in the process of RNA folding.[3–5] Tertiary compaction into dense functional structures requires much higher concentrations of $Mg^{2+}$for sufficient screening of the phosphate groups.[6] Because secondary structure can be stable independent of tertiary structure, RNA passes through collapsed

**Corresponding author.* Department of Chemistry, University of Chicago, Chicago, Illinois 60637, USA.
E-mail address: nfschere@uchicago.edu.

Present address: K. T. Lee, Korea Research Institute of Chemical Technology, Daejeon 305-343, Korea.

Abbreviations used: C_{thermo}L18, catalytic domain of RNase P RNA from *Bacillus stearothermophilus* labeled with a FRET pair on the 3′ end and L18 loop; FRET, fluorescence resonance energy transfer; E_{FRET}, efficiency of resonance energy transfer.

structures along the folding pathway that contain some secondary structure, but minimal tertiary structure.[4,7] These collapsed states are intermediate between an electrostatically self-repelling structure, and the compact native state.[4,5,7–10]

Some non-equilibrium RNA folding studies have demonstrated that when folding begins from an ensemble of collapsed structures, the dominant folding pathway depends strongly on the initial ionic strength conditions under which the collapsed RNA is pre-equilibrated.[11,12] The collapsed structures are, therefore, important in the early folding steps of large RNAs,[2,5,7,13] and strongly determine the subsequent sequence of structure formation. Hence, characterizing the equilibrium conformational dynamics and free energy surface(s) of these collapsed structures at low ionic strength can reveal critical aspects of tertiary RNA folding.

Single-molecule studies allow transcending ensemble averaged measures of behavior. Previous single-molecule RNA folding studies have found heterogeneity in equilibrium structural dynamics that are not identifiable in the ensemble.[11,14–27] Studies of the four-way hairpin ribozyme,[14,15] and the tetraloop-receptor[16] showed that even a loop docking interaction can yield significant heterogeneity in the dynamics. These studies did not establish whether the heterogeneity was static (i.e., long-lived for each molecule) or dynamic (i.e., with a time-dependent rate constant). However, the two-way junction hairpin ribozyme was observed to have long-lived (e.g., hours timescale) memory effects attributed to a loop–loop interaction.[17–19] By contrast, the four-way junction exhibits quite homogeneous dynamics and therefore little variability in structural adjustment during conformational switching.[14] The range of dynamics in these smaller RNAs is shared by larger RNA molecules.[11,20] These congruent observations support the premise that RNA dynamics are hierarchical, in part because individual structural elements retain their dynamics in folded molecules.

In this study, we investigate the dynamics of single molecules of a 260 nt RNA under conditions of electrostatic collapse but far from the native folded conformation. Previous small-angle X-ray scattering (SAXS) studies of this ribozyme, the (independently folding) catalytic domain of RNAse P from *Bacillus stearothermophilus* (C_{thermo}, Fig. 1), have shown that the unfolded state of C_{thermo} undergoes gradual Mg^{2+}-driven compaction between 0.001 mM and 0.1 mM $Mg^{2+}$with a 20% decrease in the radius of gyration, R_g, from 78 Å to 60 Å.[28] The RNA forms a tremendous amount of structure in a cooperative fashion in the subsequent folding transition (around 1 mM Mg^{2+}) to the catalytically active native state, as determined by chemical protection assays.[28–30]

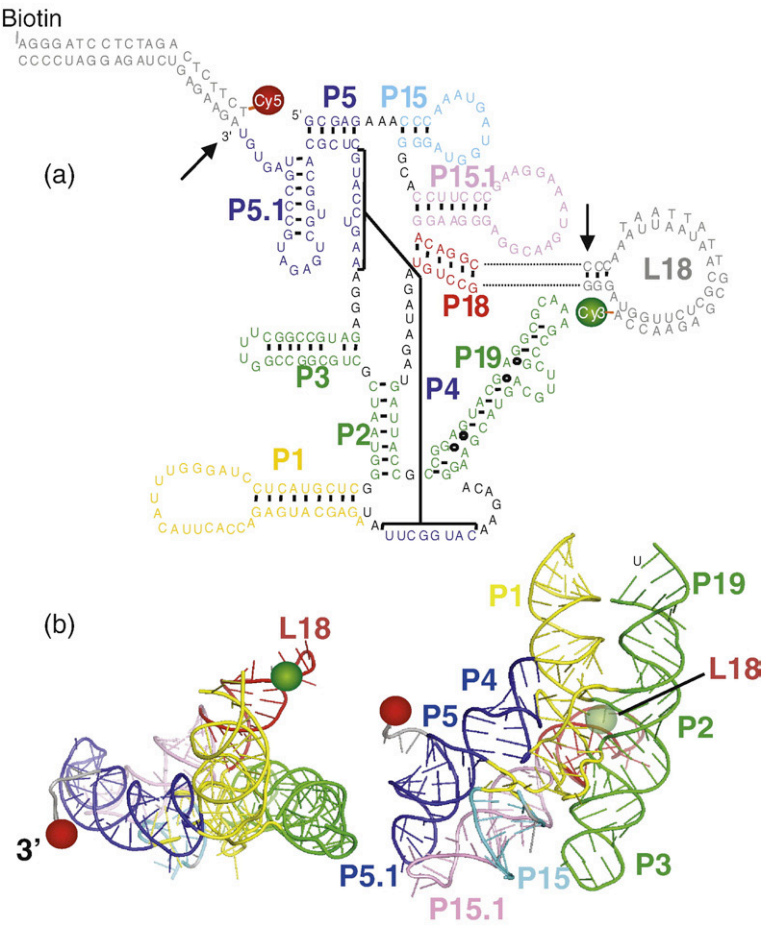

Fig. 1. (a) Secondary structure representation for the catalytic domain of RNase P RNA from *Bacillus stearothermophilus*, (C_{thermo}). C_{thermo}L18 structural modifications that allow introduction of a Cy3/Cy5 FRET pair by hybridization to the 3′ terminus and L18 loop are shown in gray. (b) Approximate (three-dimensional) position of the Cy3 (green spheres) and Cy5 (red spheres) dyes are shown in the tertiary structure representation taken from Ref. 32.

We study the structural dynamics of C_{thermo} by fluorescence resonance energy transfer (FRET) between the 3′ end and the L18 loop of C_{thermo}, termed C_{thermo}L18.[31] The labeled regions do not form tertiary interactions,[32] but they are sensitive to the formation of structures elsewhere in the RNA at all concentrations of Mg^{2+}studied. This is readily apparent in single-molecule FRET trajectories measured at different points (i.e., thermodynamic conditions) along the Mg^{2+}titration. We find that the pre-native collapsed C_{thermo} RNA fluctuates between two discrete states that have FRET values different from the fully folded structure at 1 mM Mg^{2+}. The dynamics of conformational fluctuations for individual molecules are consistent with single-exponential kinetics, suggesting a simple two-state description. However, the dwell time distributions accumulated over all molecules at a given [Mg^{2+}] show the presence of a second exponential time constant for both low and high E_{FRET} states. Together with findings from a non-equilibrium single molecule study of C_{thermo}L18,[33] we conclude that a "hidden degree of freedom" affects the observed RNA structural transition. A surprisingly simple four-state hidden Markov model is sufficient to describe these collapsed-state RNA structural transitions.[34]

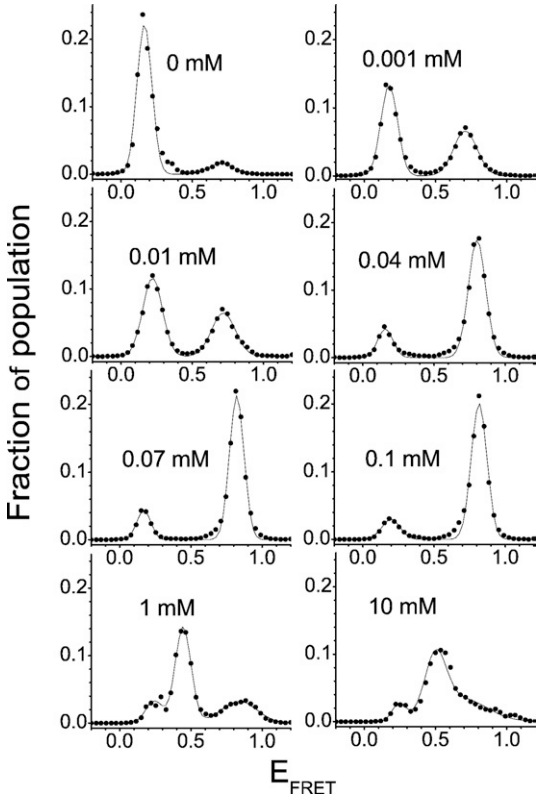

Fig. 3. Monotonic shift in the cumulative E_{FRET} histograms shows that higher [Mg^{2+}] favor more compact states. At low [Mg^{2+}] (0.001–0.1 mM, 20 mM Tris–HCl, pH 8.1), two E_{FRET} states are populated. The mid (0.45) E_{FRET} state appears only at concentrations of Mg^{2+}above 0.1 mM.

Results

Single molecule trajectories show a [Mg^{2+}]-dependent evolution of structure

Representative individual trajectories (Fig. 2a) and FRET efficiency histograms (FRET efficiency is defined as the fraction of total fluorescence due to the acceptor Cy5 fluorophore, $E_{FRET}=I_A/(I_D+I_A)$) constructed from these individual trajectories (Figs. 2b and 3) show that the conformational dynamics associated with the Mg^{2+}titration of C_{thermo}L18 can be divided into two regimes. In the low [Mg^{2+}] regime ($0 \approx 0.1$ mM, where [Mg^{2+}] ≈ 0 mM was measured in 20 mM Tris–HCl, pH 8.1 without added Mg^{2+}or chelator), the conformational fluctuations of

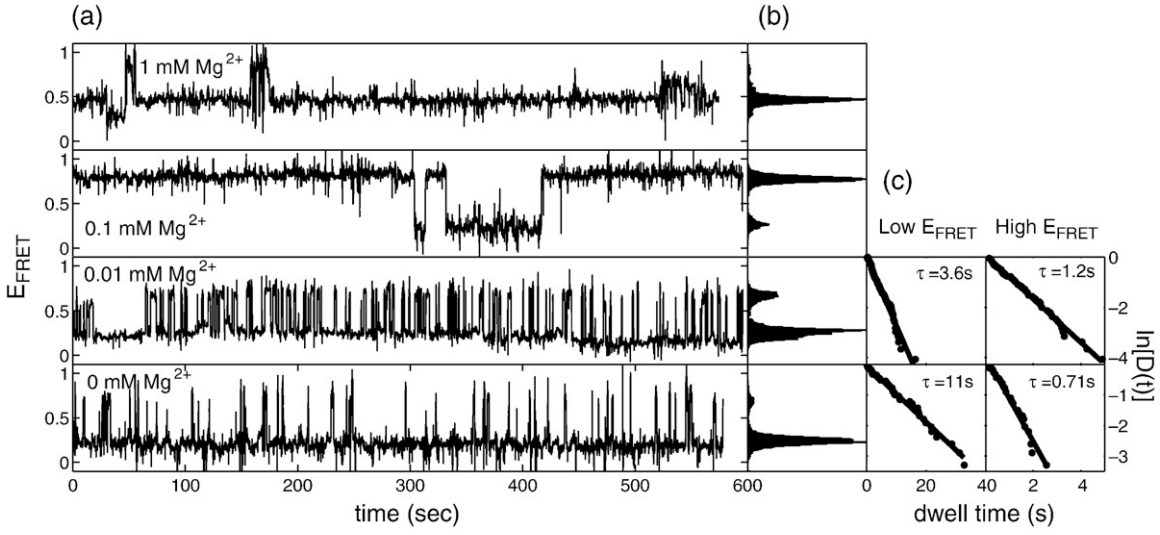

Fig. 2. Behavior of individual C_{thermo}L18 molecules. (a) Representative single molecule E_{FRET} trajectories at varying [Mg^{2+}], 20 mM Tris–HCl, pH 8.1. (b) Corresponding E_{FRET} histograms. (c) At concentrations of Mg^{2+} below 0.1 mM, the dwell times of two-level E_{FRET} trajectories with >20 transitions can be fit to a single-exponential decay.

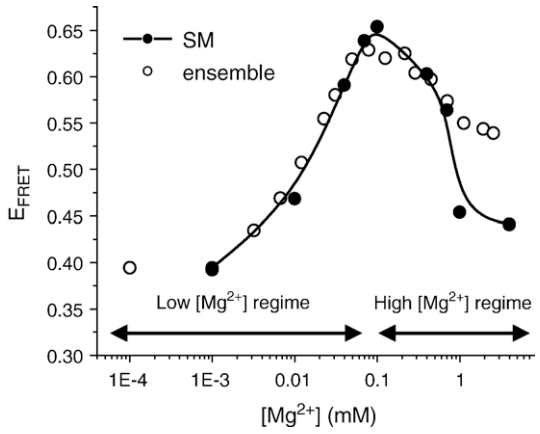

Fig. 4. Averaged E_{FRET} signal from (●) single molecule E_{FRET} histograms or from (○) solution ensemble measurement as a function of [Mg^{2+}] (in 20 mM Tris–HCl, pH 8.1). The titration is divided into low and high [Mg^{2+}] regimes, according to the single molecule behavior (two-state or multistate, respectively).

C_{thermo}L18 are two-state, with discrete jumps (with a transition time <50 ms) between low and high E_{FRET} states (E_{FRET} 0.2 and 0.8), while in the high [Mg^{2+}] regime (i.e., 0.1 to 1 mM), the conformational fluctuations are multi-state and more complex.

The two [Mg^{2+}] regimes are distinguished by characteristically different structural transitions. In the low [Mg^{2+}] regime, the E_{FRET} population shifts gradually and monotonically from the low E_{FRET} 0.2 state to the high E_{FRET} 0.8 state. In the higher [Mg^{2+}] regime, the multiple populations evolve in a complicated manner, ultimately shifting to a state with E_{FRET} 0.45. Figure 4 shows the changes in average E_{FRET} value at each [Mg^{2+}] that reflect these two major structural transitions; $\langle E_{FRET} \rangle$ increases in the low [Mg^{2+}] regime, and $\langle E_{FRET} \rangle$ decreases in the high [Mg^{2+}] regime. The titration curve shows clearly that the low [Mg^{2+}] regime transition takes place over more than a 1000-fold range in [Mg^{2+}], while the high [Mg^{2+}] regime transition takes place within a tenfold range in [Mg^{2+}]. The mechanisms of these two transitions are likely to be quite different and are discussed below. However, our focus is on the low ionic strength conditions in which C_{thermo}L18 behaves in a two-state manner.

Individual molecule dwell time analysis

We used FRET to determine transition rates for each molecule by extracting dwell times, the length of time spent in a single E_{FRET} state, from the trajectories. For individual molecules that undergo >20 transitions within the observation window (5–10 min), dynamics of the low and high E_{FRET} states can be analyzed as described to determine the E_{FRET} state lifetimes.[20] The dwell time distribution, here defined as:

$$D(t) = 1 - \frac{1}{N}\sum_{t_i<t} p(t_i),$$

where N is the total number of dwell times and $p(t_i)$ are the number of dwell times with length t_i, is plotted for individual molecules in Fig. 2c. The logarithm of the dwell time distribution, ln[$D(t)$], was used for weighting purposes. We find that dwell time distributions for individual molecules fit well to single exponentials, yielding the microscopic transition time constants, τ_l and τ_h, for the two-state model:

$$low\ E_{FRET} \underset{\tau_{h,i}}{\overset{\tau_{l,i}}{\rightleftharpoons}} high\ E_{FRET},$$

where the subscript i enumerates each single molecule.

Although each molecule obeys well-defined two-state kinetics, the collection of microscopic time constants shown in Fig. 5, demonstrates that there is molecule-to-molecule variation in their kinetics with no correlation between τ_l and τ_h. The scatter in τ_l and τ_h is small; e.g., it is comparable to the relatively narrow and homogeneous distributions observed for the 4H junction[14] or the nanometronome.[35] Inspection of individual E_{FRET} trajectories indicates that some of this variation cannot be explained by sampling-based statistical variation. In particular, the outliers maintain a persistent behavior; slowly fluctuating molecules remain slow while rapidly fluctuating molecules remain rapid (see Fig. 6, 0.01 mM Mg^{2+}). This result is similar to the heterogeneity observed in the distribution of average dwell times per molecule for the hairpin ribozyme.[14] Thus, individual molecules follow a well-defined two-state kinetic scheme within the observation window. This small but persistent variation in individual rate constants suggests that the structural change probed by the 3′-L18 label pair is sensitive to slow conformational changes. These changes are "hidden", in that they do not change the E_{FRET} values but alter the dynamics sampled by the RNA

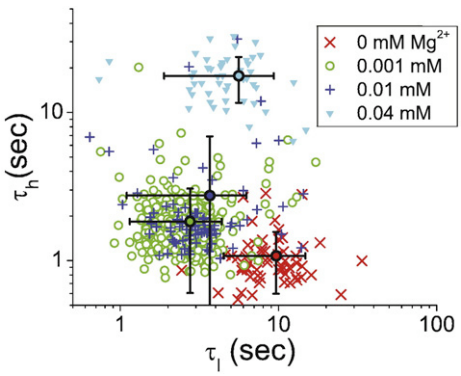

Fig. 5. [Mg^{2+}]-dependent changes in average $\tau_{l\text{-fast}}$ (low E_{FRET} state time constants) and $\tau_{h\text{-fast}}$ (high E_{FRET} state time constants) determined from single-exponential fits to individual dwell time histograms. Each symbol (×, ○, +, ▼) corresponds to rate constants from a single molecule, and shows that the transition rates are distributed in an uncorrelated manner. Large filled circles indicate the mean value of individual rate constants with standard deviation shown as black error bars.

structure on the minutes timescale. Similar slow conformational changes have been attributed to slow interconversion of alternate loop configurations in the minimal active form of the hairpin ribozyme.[17–19]

Cumulative dwell time analysis

Distributions of dwell times for each E_{FRET} state accumulated over >250 individual molecules at each condition establish the relaxation properties of the entire population. The resulting distributions, *D(t)*, constructed in the same manner as the individual dwell time histograms described above, display dwell times extending over three decades from 100 ms to >100 s. These (decay) histograms fit well to a double exponential (Fig. 7b and c). Single or stretched exponentials give poorer fits as measured by the residuals (Fig. 7a). The fast components of the double exponentials ($\tau_{l\text{-fast}}$ and $\tau_{h\text{-fast}}$) dominate the fits with >80% amplitude at nearly all concentrations of Mg^{2+}.

The exponential time constants, $\tau_{l\text{-slow}}$, $\tau_{l\text{-fast}}$, $\tau_{h\text{-slow}}$, and $\tau_{h\text{-fast}}$, depend on $[Mg^{2+}]$ (Fig. 8a and b) as is required by the observed population shift favoring the high E_{FRET} state at increased $[Mg^{2+}]$ (Fig. 3). Although all time constants increase from 0.01 mM to 0.1 mM Mg^{2+}, $\tau_{h\text{-fast}}$ increases by a factor of 51, while the $\tau_{l\text{-fast}}$ increases only by a factor of 6. This asymmetry results from increased stabilization of the high E_{FRET} state relative to the low E_{FRET} state. We note that although the τ_l and τ_h time constants generally decrease with decreasing $[Mg^{2+}]$, at ≈0 mM $Mg^{2+}$the time constants for the low E_{FRET} state are larger than at 0.001 mM Mg^{2+}(see Figs. 5 and 8). This non-monotonic behavior may be due to experimental limits in time resolution (i.e., high E_{FRET} dwell times are so short that they are not detected, increasing the apparent dwell time in the low E_{FRET} state), or may indicate a structural transition. Further studies are required to resolve the origin of this result.

The mean values of the time constants of the individual molecule results at each $[Mg^{2+}]$ (heavy filled circles in Fig. 5) are plotted in Fig. 8a and b (black crosses). The mean values are in excellent agreement

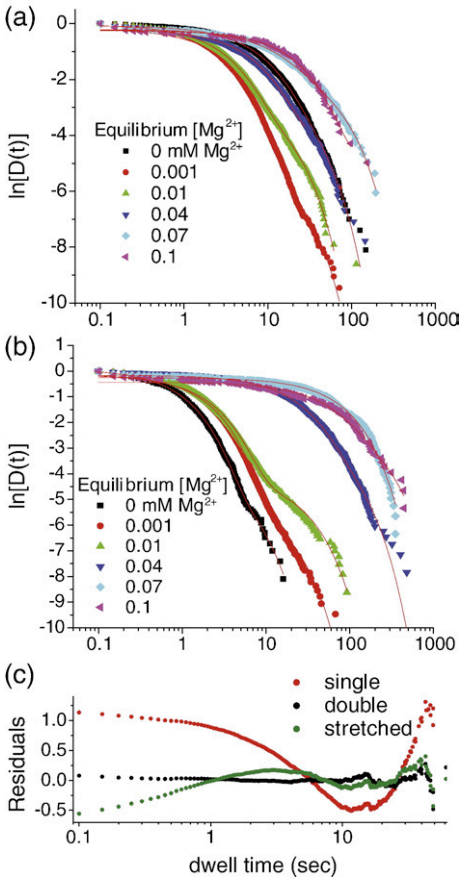

Fig. 7. Dwell-time distributions (ln[D(t)]) *versus* log time) accumulated over all (>250) trajectories at a given $[Mg^{2+}]$ for the low E_{FRET} (a) and high E_{FRET} states (b). For weighting purposes:

$$\ln[D(t)] = \ln\left[1 - \frac{1}{N}\sum_{t_i<t} p(t_i)\right]$$

was fit to the natural logarithm of a double exponential and is shown on a log–linear scale. (c) Comparison of residuals for single (red), double (black), and stretched (green) exponential fits to the low E_{FRET} dwell time histogram at 0.01 mM Mg^{2+} (note the different time axis range).

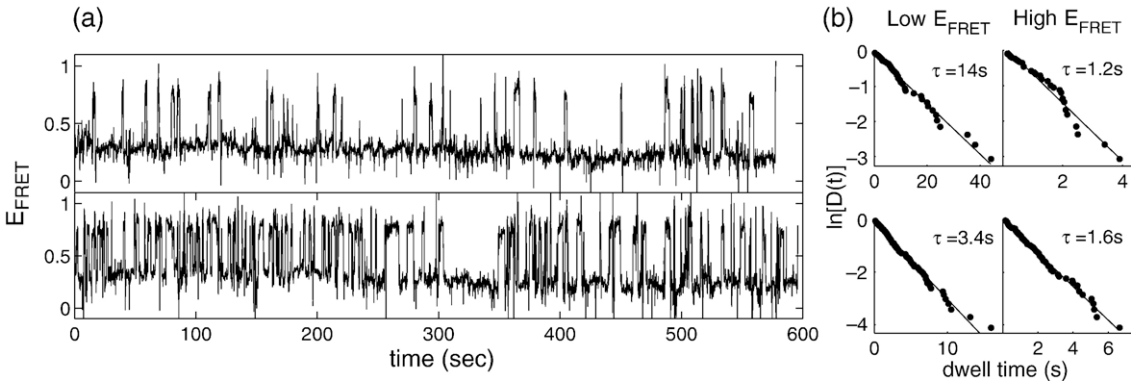

Fig. 6. Two trajectories at 0.01 mM Mg^{2+}, 20 mM Tris–HCl (pH 8.1) demonstrate static heterogeneity: the dynamics of some molecules are slow (top) while dynamics of other molecules are fast (bottom) for the duration of the measurement. Individual molecule dynamics are characterized by well-defined barriers that do not change on the observation timescale.

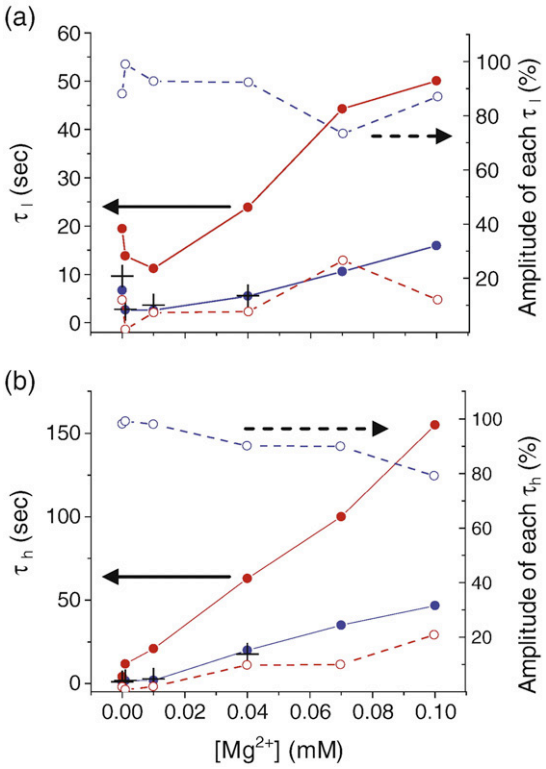

Fig. 8. Double-exponential fit parameters $\tau_{l\text{-slow}}$, $\tau_{l\text{-fast}}$ (a) and $\tau_{h\text{-slow}}$, $\tau_{h\text{-fast}}$ (b) (●, left-hand axis) vary with $[Mg^{2+}]$ (20 mM Tris–HCl, pH 8.1). Fast time constants are blue, slow time constants are red. The fast time constant dominates all dwell time distributions, as can be seen from the percentage amplitude of each component (○, right-hand axis). The average time constant (black+) determined from single exponential fits to individual molecule dwell time histograms (see Fig. 5) is superimposed, showing agreement.

with the fast time constants, $\tau_{l\text{-fast}}$ and $\tau_{h\text{-fast}}$. Dwell times associated with the slow dynamics, $\tau_{l\text{-slow}}$ and $\tau_{h\text{-slow}}$, are rare so that, in general, the slow time constants cannot be measured for individual molecules under current experimental conditions unless the slow time constants are sufficiently fast, as shown in Fig. 6. The amplitude of the slow component in the cumulative dwell time histograms is small, so that only a fraction of all dwell times arise from the slow time constants. Additionally, even if a molecule's dynamics were governed by a slow time constant for a significant portion of a trajectory, the number of dwell times observable within the 5–10 min trajectory length (which is determined by the photobleach lifetimes of the Cy dyes) is insufficient for fitting to a single exponential.

The cumulative dwell time distributions for both the low and high E_{FRET} states exhibit biexponential dynamics implying a minimum of two low and two high E_{FRET} substates (Fig. 9a).[34] A three-state model is not possible because the singly degenerate state would yield single-exponential kinetics with a time constant equal to the sum of the two transition time constants associated with leaving the singly degenerate state. Higher-order consecutive dwell time correlations are consistent with the four-state model (data not shown), although we cannot rule out the existence of other hidden states with low amplitude (i.e., rare conformations) or similar time constants as those measured.[36] Furthermore, despite the large sample size, we are not able to specify the connectivities of states (see[37] and references therein for a discussion of information extraction and model building).

Although a specific kinetic model for the observed E_{FRET} state behavior is not accessible without greater sampling of the dwell times that arise from the slow dynamics, the double exponential rather than stretched-exponential kinetics allow us to suggest the most plausible models. The RNA structure may rapidly sample the many shallow wells defined by weak interactions that one would presume exist in the collapsed region of the energy landscape. However, the simple exponential kinetics that we observe rather than stretch exponential (or power law) kinetics suggest that only a very few states and barriers actually define the folding landscape. This presumably follows from energy scale separation of the interactions/contacts that form. This is quite remarkable considering the size of C_{thermo}L18 and the large number of possible stabilizing interactions available. Presumably, the energetics of the alternative interactions are much lower than the observed stable states so that their influence on the dynamics is averaged out on the measurement timescale. C_{thermo}L18 does

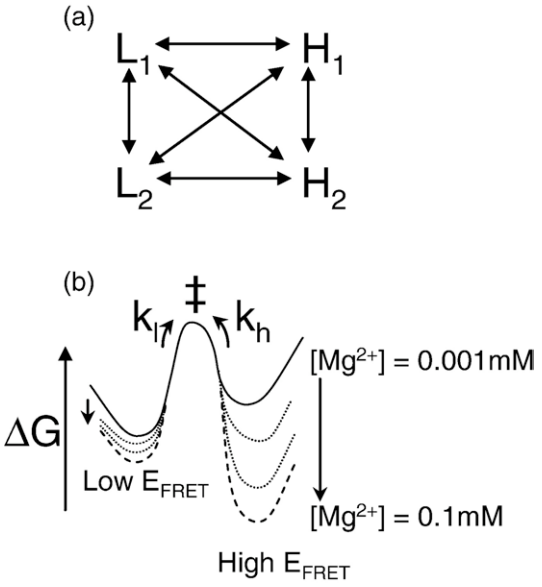

Fig. 9. (a) Double-exponential components in both low and high E_{FRET} dwell time histograms require two or more substates with low or high E_{FRET} signals. Shown here is a minimal model that fulfills this requirement, although there may be other hidden substates that are undetected in our experiments and not all interconversions (arrows) need be present in the underlying model. (b) Schematic of the $[Mg^{2+}]$-dependent changes in the free energies of the low and high E_{FRET} states relative to the transition (‡) state. The low E_{FRET} state is stabilized by only a small degree with increased $[Mg^{2+}]$, while the high E_{FRET} state becomes significantly more stable.

not display dynamic heterogeneity; instead, individual molecules maintain well-defined kinetics within a trajectory. This is unlike the heterogeneity observed in RNA systems in which the interaction being studied is a loop–receptor interaction.[14–17,19,]

Discussion

C_{thermo}L18 E_{FRET} fluctuations are sensitive to collapse at low [Mg^{2+}] and cooperative folding at high [Mg^{2+}]

C_{thermo} is known to undergo two types of structural changes during equilibrium folding: a gradual global collapse at low [Mg^{2+}], and a cooperative structural transition at higher [Mg^{2+}].[28–30] Both transitions are observed in the present single-molecule study of C_{thermo}L18. Fig. 10 shows that in the low [Mg^{2+}] regime, the FRET signals increase slightly with increasing [Mg^{2+}], presumably due to non-specific electrostatic compaction. In addition to this continuous (small) E_{FRET} value shift, increasing [Mg^{2+}] also shifts the RNA population from a discrete low E_{FRET} 0.2 state to a more collapsed but non-native high E_{FRET} 0.8 state. The discrete nature of this global collapse has not been reported.

In the high [Mg^{2+}] regime (>0.1 mM Mg^{2+}), the cooperative transition to the native state is observed in C_{thermo}L18 as the introduction of new E_{FRET} states. The new E_{FRET} 0.45 state that dominates trajectories at 1.0 mM Mg^{2+}corresponds to an inter-dye distance of approximately 60 Å (assuming $\kappa = 2/3$[38]), in good agreement with the 3-L18 distance one can determine from the crystal structure (Fig. 1b).[32] In summary, the dyes in the high E_{FRET} (0.8) state are closer than they would be in the native structure. Presumably, the formation of some native tertiary structure, e.g. the P2-P4 pseudoknot, results in a slight separation of the dye pair.

Structure of low and high E_{FRET} states

The native (crystal) structure of the full-length RNase P RNA[32] (Fig. 1b) provides a starting point for interpreting the dynamics observed in C_{thermo}L18.

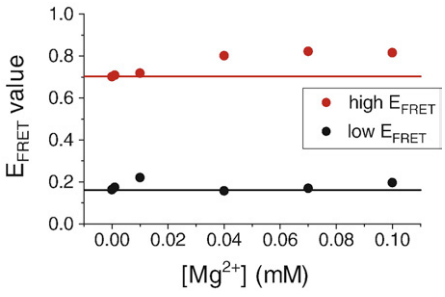

Fig. 10. A slight increase in average E_{FRET} value for the low (black) and high (red) E_{FRET} states as a function of [Mg^{2+}] is consistent with electrostatic collapse. Noise is due to variability of background subtraction for individual molecules.

There are two major stabilizing interactions in this RNA: (*i*) docking between loops L5.1 and L15.1; and (*ii*) the catalytic core, a complex central structure that pulls together the stems by arranging junction regions in a network of non-canonical interactions. We believe that topological constraints of the native state require formation of the following helices: P4 first, then P2, then finally P5, with a number of non-canonical stabilizing interactions in the catalytic core. Formation of these helices in different order or combinations may result in intermediate states that are kinetically stable. In the following discussion of a possible structural context for the observed E_{FRET} states and dynamics, any number interactions can be hypothesized, but we will restrict ourselves to discussion of the stabilizing interactions observed in the crystal structure.

Polynucleotides generally obtain their structure by maximizing base pairing while minimizing the electrostatic repulsion.[39] For both the low and high FRET states, we assume that the local helices P5.1, P3, P1, P19, P18, P15.1, and P15 are formed (Fig. 1a).[4,5] The dyes at the 3′ end and the L18 loop are tethered by the intervening RNA strand with an effective single-stranded length of ~70 nt, where the effective single strand consists of the residues outside of Watson–Crick base-paired regions plus two residues for each base-paired stem (Fig. 1a). The E_{FRET} 0.2 state is comparable to the E_{FRET} value determined for a 70 nt single-stranded poly(dT).[40,41] This suggests that the simplest model for the low E_{FRET} state of C_{thermo}L18 contains just these local helices and an effective single-stranded tether of ~70 nt separating the Cy3/Cy5 FRET pair.

The E_{FRET} 0.8 state corresponds to an inter-dye distance of ~50 Å, which is shorter than the ~60 Å (expected $E_{FRET} \approx 0.5$) separation observed in the crystal structure. A shorter inter-dye distance, together with a [Mg^{2+}]-dependent population shift favoring the high E_{FRET} state, implies that non-local structure is formed in the high E_{FRET} (0.8) state. Among the three long-range helices, P2, P4, and P5, formation of either P2 or P4 alone will not bring the dyes close enough to give a 0.8 E_{FRET} signal. P5, however, could position the L18 loop within 50 Å of the 3′ end if one assumes the chain is free to undergo movement. Formation of other tertiary structures in the native state presumably reduce the rotational orientations of the helices (dyes) and force them further apart. Further studies are required to test whether the formation of P5 is indeed responsible for the E_{FRET} 0.8 state.

The gradual two-state population shift in the low [Mg^{2+}] regime (Figs. 3 and 4) is consistent with these suggested structures of the low and high E_{FRET} states. In an ensemble experiment, the low [Mg^{2+}] regime of the E_{FRET} titration curve (Fig. 4) would be fit to a two-state Hill model, yielding a small Hill coefficient of 1.4.[42] Such non-cooperative behavior has been shown to characterize the formation of non-native intermediate structures in the collapsed states for other large RNAs, such as the bI5 core,[7] *Tetrahymena* ribozyme,[43] as well as formation of the isolated tetraloop–tetraloop receptor interaction.[16]

A small Hill coefficient may reflect uncorrelated transitions, which would be consistent with our observation that the hidden degrees of freedom do not alter the E_{FRET} values.

The simplest description of structural dynamics at low [Mg^{2+}] is that the various structural motifs (stems, loops, single-stranded regions) of C_{thermo}L18 move relatively independently. For [Mg^{2+}] >0.1 mM, a multi-state search for the fully folded state (Fig. 2a) replaces the two-state behavior. With greater charge shielding and increased binding of Mg^{2+}, the independent motions of structural components that stabilize the fully folded state can be expected to become more concerted and cooperative.[32] Close coordination of the motions of several structural elements is a plausible requirement for formation of the pseudoknot core and thereby narrows the conformational search at high [Mg^{2+}].[44] Thus, the C_{thermo}L18 RNA folding titration can be characterized as a transformation from non-cooperative to cooperative structural changes. Changing the probe placement may allow observation of different behaviors or other aspects of the overall conformational change. Work is ongoing to investigate this issue.

Characteristics of the free energy surface

The Mg^{2+}-dependence of individual molecule time constants (τ_l and τ_h), E_{FRET} state population shifts, and cumulative dwell time histogram time constants yield the picture of relative free energies of the low E_{FRET}, high E_{FRET}, and transition states shown in Fig. 9b. Because we measure microscopic rate constants that directly reflect the forward and reverse barrier heights but do not measure the absolute free energy of any state, it is convenient to represent the changes in the free energy surface relative to a fixed barrier height. (Of course, this kinetic scheme is isomorphic with one in which the free energy of the open state is held fixed and both the barrier height and the stability of the closed state are increased as [Mg^{2+}] increases.) Firstly, the population shift with increasing [Mg^{2+}] favoring the high E_{FRET} state indicates that its free energy is stabilized significantly relative to the low E_{FRET} state. Secondly, τ_l increases by a factor of 6 between 0.001 mM and 0.1 mM Mg^{2+} (Fig. 8) whereas τ_h increases by a factor of 51. The free energy of the low E_{FRET} state, therefore, is stabilized to only a small degree relative to the barrier, while the high E_{FRET} state is stabilized by another factor of 8.

Stabilization of both low and high E_{FRET} states (relative to the transition state) with increasing [Mg^{2+}] is unusual among single-molecule RNA folding studies. A number of systems show only stabilization of the high E_{FRET} (compact) state with destabilization of the low E_{FRET} (open) state (See Table 1 for a summary of time constants). For example, over the range from ≈0 to 0.1 mM Mg^{2+}, the three-helix junction,[23] GAAA tetraloop-receptor motif,[16] four-way hairpin ribozyme,[14] and two-way hairpin ribozyme,[18] all stabilized the closed state and destabilized the open state relative to the transition state. On the other hand, the 4H junction stabilized both the low and high E_{FRET} conformations equally,[14] and the nanometronome stabilized both conformations nearly equally.[35]

The explanation given for simultaneous stabilization of the low and high E_{FRET} states in the 4H junction and nanometronome may be applicable to C_{thermo}L18. If Mg^{2+}stabilizes one E_{FRET} state, the immediate implication is that the structure is collapsed. Electrostatic repulsion tends to destabilize close contacts at low ionic strength so increasing [Mg^{2+}] allows better charge shielding. If increased [Mg^{2+}] increases the barrier height, then the barrier crossing must involve some Mg^{2+}dissociation, which is unfavorable at higher [Mg^{2+}]. The low and high E_{FRET} states of C_{thermo}L18 are both stabilized relative to the transition state with increasing [Mg^{2+}], and

Table 1. [Mg^{2+}]-dependence of the two-state time constants (t_{closed}, t_{open}) of previously described nucleic acid structural motifs

Nucleic acid structural motif featuring two-state dynamics		[Mg^{2+}] ≤0.001 mM	[Mg^{2+}] ~0.1 mM	Change (%)	Observed heterogeneity?
Three-helix junction [23]	τ_{closed} (ms)	2	12	600	Yes
	τ_{open} (ms)	37	14	38	
GAAA tetraloop-receptor motif [16]	τ_{closed} (s)	0.097	0.130	134	Yes
	τ_{open} (s)	0.20	0.095	47	
Two-way hairpin ribozyme [18]	τ_{closed} (s)	3	10	333	Yes
	τ_{open} (s)	50	3.3	7	
Four-way hairpin ribozyme [14]	τ_{closed}	Individual time constants not reported		>100	Yes
	τ_{open}			<100	
4H junction [14]	τ_{closed}	Individual time constants not reported		Increased equally	No
	τ_{open}				
Nanometronome [35]	τ_{closed} (s)	0.7	7	1000	No
	τ_{open} (s)	0.1	0.7	700	
C_{thermo}L18 RNA	τ_{closed} (s)	2.6	15.9	610	No
	τ_{open} (s)	0.9	46.6	5170	

The percentage change of time constants with increasing [Mg^{2+}] (($\tau_{0.1mM}/\tau_{0mM}$)×100%) is given in the fifth column. The qualitative trend in time constants for the four-way hairpin ribozyme and 4H junction are included rather than individual rate constants because only the sum of rate constants was reported by Tan *et al.*[14] The last column lists reported heterogeneity of the time constants, which we define as deviation from exponential behavior.

are therefore both likely to be collapsed to some degree, with the transition between states requiring Mg^{2+}dissociation. Although our FRET pair reports only on the collapsed nature of the high E_{FRET} state (by definition, a high E_{FRET} signal implies that the FRET dyes are close together, a low E_{FRET} signal implies the FRET dyes are further apart), our results predict that the low E_{FRET} state is collapsed in a region of the RNA not probed by the 3′-L18 FRET pair.

The homogeneity of time constants in the nanometronome supports the suggestion that the high E_{FRET} state in C_{thermo}L18 involves formation of a base-pairing interaction. The homogeneity of kinetics in C_{thermo}L18 are similar to the homogeneity of kinetics for the sticky ends in the nanometronome and in the base-pairing of molecular beacons,[45] and unlike loop–receptor interactions. Formation of the P5 helix in the high E_{FRET} state is a reasonable proposal for the interaction that describes the "observed" degrees of freedom.

Conclusion

For the $[Mg^{2+}]$-dependent low-to-high E_{FRET} transition studied here, the simple picture of a monotonic shift from an open to a closed structure, suggested by the ensemble averaged behavior, masks structural complexities apparent from analysis of single-molecule dynamics and kinetics. Both the low and high E_{FRET} states observed in the low $[Mg^{2+}]$ range studied are likely to contain collapsed substructures that are stabilized by non-specific ction shielding; both states become more stable relative to the transition state with increasing $[Mg^{2+}]$. Homogeneity of time constants suggests that the high E_{FRET} state most likely includes formation of a long-range helix with canonical base-pairings. Double-exponential fits to cumulative dwell time distributions suggest that the two observed E_{FRET} states probe one major structural interaction, but that other structural interactions that are hidden from the 3′-L18 FRET pair affect the dynamics of the observed states. The minimal model required to encompass all observations is a four-state Markovian model, as shown in Fig. 9a.

Large RNAs at low ionic strength generally exhibit chemical protection patterns that indicate the absence of stable tertiary structure.[2] This fact and previous small-angle X-ray scattering measurements of the C-domain,[28] and other RNAs[8,9] have suggested that RNA intermediates can exist as a relaxed ensemble with well-defined secondary but ill-defined tertiary structure. In this view, the RNA conformational free energy surface contains only very shallow ripples of energy difference between conformations. An observation of discrete well-defined conformations in C_{thermo}L18 that are stable on the seconds timescale at low $[Mg^{2+}]$ suggests that even at low ionic strength, with a tremendous number of possible (weak) interactions, a few critical interactions may produce deep energy wells and the resulting kinetics are relatively simple.

Given the hierarchical nature of the interactions and secondary structure formation in RNA *versus* the "even keel" energetics in protein folding (i.e., many interactions including the hydrophobic effect, solvation, electrostatics, H bonding, etc. are similar in magnitude), one might suppose that the dynamics (hence energy landscape) would also be different in proteins and RNA. However, simple structural dynamics are consistent with the exponential kinetics observed in the folding of most small proteins.[46] Synnergies or cooperativity of apparently distinct driving forces may be the key. The simplicity of the kinetics we observe suggests a "landscape" or kinetic scheme as shown in Fig. 9 for collapsed state dynamics: a single dominant barrier for the observed degree of freedom (3′-L18 distance) but sensitivity to conformations and structures of other parts of the ribozyme that we term hidden. Figures 3 and 4 show that these hidden conformations/structures eventually do affect the E_{FRET} states (values) and their populations at high $[Mg^{2+}]$ and in non-equilibrium periodic $[Mg^{2+}]$-jump experiments.[33]

Finally, an intriguing possibility is that the simple dynamics observed are related to the fact that this ribozyme folds in a highly cooperative manner (Hill coefficient of 7.8).[28] Our earlier single-molecule study of a similar ribozyme but from a mesophilic organism, whose folding is not as cooperative (Hill coefficient 2.9),[12] showed more complex and inhomogeneous kinetics, as would be expected from a more complex energy landscape.[27] It would be interesting and important to know if simple (exponential) kinetics in the pre-transition region are a hallmark or even a necessity for highly cooperative transitions and folding. These studies are in progress.

Materials and Methods

RNA preparation

The catalytic domain of RNase P RNA from *Bacillus stearothermophilus*[47] was prepared by standard *in vitro* transcription and labeled with FRET donor and acceptor molecules Cy3 and Cy5, respectively, by an oligonucleotide hybridization method.[31] The catalytic domain sequence was modified to allow site-specific fluorophore labeling by extending the 3′ end, and by replacing loop 18 (C_{thermo}L18) with a hybridization target sequence (Fig. 1). Cy3-labeled and Cy5 and biotin-labeled DNA oligonucleotides were purchased from IDT. This labeling method has been shown to be an efficient method of incorporating FRET pairs on RNA molecules without perturbing the folding pathway and catalytic activity.[31,48]

Single-molecule E_{FRET} measurements

Single-molecule experiments were performed by immobilization of biotinylated C_{thermo}L18 RNA on a coverslip sparsely functionalized with streptavidin and coated with a lipid bilayer.[49] A perfusion chamber gasket (SA50, Grace Bio-Labs) allowed the buffer to be exchanged. Coverslips were cleaned with Pirhana solution (30% H_2O_2/H_2SO_4, 1:3, v/v), exposed to 0.02 mg/mL streptavidin (Invitrogen,

S888) in 20 mM Tris for 15 min, then incubated in 1 mg/mL DPTC lipid in 5 mM Tris, 50 mM NaCl, 0.5 mM EDTA for 1 h.[49,50,51] C_{thermo}L18 was immobilized by incubating the lipid bilayer-coated coverslips in 500 pM RNA (20 mM Tris (pH 8), 0.01 mM Mg^{2+}) for 20 min. The RNA was then equilibrated for 20 min at the desired [Mg^{2+}] in 20 mM Tris before imaging. Fluorescence trajectories of surface-immobilized RNA were collected at room temperature (18 °C) in the presence of the glucose oxidase/catalase oxygen-scavenger system:[49] 0.1 mg/mL glucose oxidase, 0.04 mg/mL catalase, 1.5 mM Trolox, and 4 mg/mL glucose. Single-molecule E_{FRET} time trajectories with 50 ms frame integration time were collected with an objective-based total internal reflection fluorescence microscope (Semrock FF545/650 primary dichroic, Chroma 645DCXR secondary dichroic, and Chroma bandpass filters HQ590/60M and HQ690/60M), and imaged onto an electron multiplying CCD array detector (iXon DV887-BI, Andor) with a total magnification of 150×.[52]

Trajectory analysis

Trajectories of individual molecules were extracted with an image processing routine written in MATLAB. For detection of the Cy5 photobleach event and dwell times, the trajectory noise was reduced using a non-linear predictive filter for E_{FRET} trajectories,[53] or by three-point rebinning. These methods produced indistinguishable results. The FRET efficiency along a trajectory was calculated according to:

$$E_{FRET} = I_A/(I_D + I_A)$$

where I_D and I_A are the fluorescence intensity from the donor and acceptor, respectively. [39] Digitization of the resulting two-state trajectories (high E_{FRET} and low E_{FRET} states) was accomplished by thresholding, using the minimum between the low and high E_{FRET} Gaussian peaks, equivalent to the methods used in variational transition state theory.[54]

Removing sources of heterogeneity

Earlier measurements of C_{thermo}L18, performed with the same oxygen-scavenging buffer, except that β-mercaptoethanol was used in place of Trolox, an the coverslip surface was passivated with PEG instead of a lipid bilayer, exhibited more inhomogeneous dynamics and kinetics (unpublished results). The present experiments using Trolox essentially do not have "dynamics" due to dye blinking. Furthermore, PEG-coated surfaces give rise to significant heterogeneity in the timescales of single-molecule dynamics. Without changing to a Trolox buffer and bilayer surface, the accumulated dwell time distributions shown in Fig. 7 are less clearly biexponential, such that biexponential and stretched exponential dwell time distributions are equally good descriptions of the data.

Acknowledgements

This work was supported by the National Institutes of Health (GM067961), and the Burroughs Wellcome Fund Interfaces ID 1001774 Fellowship (X.Q. and J. P.). N.F.S. thanks the John S. Guggenheim Memorial Foundation for a fellowship.

References

1. Tinoco, I., Jr & Bustamante, C. (1999). How RNA folds. *J. Mol. Biol.* **293**, 271–281.
2. Brion, P. & Westhof, E. (1997). Hierarchy and dynamics of RNA folding. *Annu. Rev. Biophys. Biomol. Struct.* **26**, 113–137.
3. Fang, X.-W., Littrell, K., Yang, X., Henderson, S. J., Siefert, S., Thiyagarajan, P. *et al.* (2000). Mg^{2+}-dependent compaction and folding of yeast tRNA and C domain of B. subtilis RNase P RNA. *Biochemistry*, **39**, 11107–11113.
4. Chamberlin, S. & Weeks, K. (2003). Differential helix stabilities and sites pre-organized for tertiary interactions revealed by monitoring local nucleotide flexibility in the bI5 group I intron RNA. *Biochemistry*, **42**, 901–909.
5. Rangan, P., Masquida, B., Westhof, E. & Woodson, S. (2003). Assembly of core helices and rapid tertiary folding of a small bacterial group I ribozyme. *Proc. Natl Acad. Sci. USA*, **100**, 1574–1579.
6. Draper, D., Grilley, D. & Soto, A. M. (2005). Ions and RNA folding. *Annu. Rev. Biomol. Struct.* **34**, 221–243.
7. Buchmueller, K. L. & Weeks, K. M. (2003). Near native structure in an RNA collapsed state. *Biochemistry*, **42**, 13869–13878.
8. Buchmueller, K. L., Webb, A. E., Richardson, D. A. & Weeks, K. M. (2000). A collapsed non-native RNA folding state. *Nature Sruct. Biol.* **7**, 362–366.
9. Russell, R., Millett, I. S., Doniach, S. & Herschlag, D. (2000). Small angle X-ray scattering reveals a compact intermediate in RNA folding. *Nature Struct. Biol.* **7**, 367–370.
10. Russell, R., Millett, I. S., Tate, M. W., Kwok, L. W., Nakatani, B., Gruner, S. M. *et al.* (2002). Rapid compaction during RNA folding. *Proc. Natl Acad. Sci. USA*, **99**, 4266–4271.
11. Russell, R., Zhuang, X., Babcock, H. P., Millett, I. S., Doniach, S., Chu, S. & Herschlag, D. (2002). Exploring the folding landscape of a structured RNA. *Proc. Natl Acad. Sci. USA*, **99**, 155–160.
12. Pan, T., Fang, X.-W. & Sosnick, T. (1999). Pathway modulation, circular permutation and rapid rna folding under kinetic control. *J. Mol. Biol.* **286**, 721–731.
13. Su, L. J., Waldsich, C. & Pyle, A. M. (2005). An obligate intermediate along the slow folding pathway of a group II intron ribozyme. *Nucleic Acids Res.* **33**, 6674–6687.
14. Tan, E., Wilson, T. J., Nahas, M. K., Clegg, R. M., Lilley, D. M. J. & Ha, T. (2003). A four-way junction accelerates hairpin ribozyme folding *via* a discrete intermediate. *Proc. Natl Acad. Sci. USA*, **100**, 9308–9313.
15. Okumus, B., Wilson, T. J., Lilley, D. M. J. & Ha, T. (2004). Vesicle encapsulation studies reveal that single molecule ribozyme heterogeneities are intrinsic. *Biophys. J.* **87**, 2798–2806.
16. Hodak, J. H., Downey, C. D., Fiore, J. L., Pardi, A. & Nesbitt, D. J. (2005). Docking kinetics and equilibrium of a GAAA tetraloop-receptor motif probed by single-molecule FRET. *Proc. Natl Acad. Sci. USA*, **102**, 10505–10510.
17. Zhuang, X., Kim, H., Pereira, M. J. B., Babcock, H. P., Walter, N. G. & Chu, S. (2002). Correlating structural dynamics and function in single ribozyme molecules. *Science*, **296**, 1473–1476.

18. Bokinsky, G., Rueda, D., Misra, V. K., Rhodes, M. M., Gordus, A., Babcock, H. P. *et al.* (2003). Single-molecule transition-state analysis of RNA folding. *Proc. Natl Acad. Sci. USA*, **100**, 9302–9307.
19. Rueda, D., Bokinsky, G., Rhodes, M. M., Rust, M. J., Zhuang, X. & Walter, N. (2004). Single-molecule enzymology of RNA: essential functional groups impact catalysis from a distance. *Proc. Natl Acad. Sci. USA*, **101**, 10066–10071.
20. Bartley, L. E., Zhuang, X., Das, R., Chu, S. & Herschlag, D. (2003). Exploration of the transition state for tertiary structure formation between an RNA helix and a large structured RNA. *J. Mol. Biol.* **328**, 1011–1026.
21. Bokinsky, G. & Zhuang, X. (2005). Single-molecule RNA folding. *Accts Chem. Res.* **38**, 566–573.
22. Ha, T., Zhuang, X., Kim, H., Orr, J. W., Williamson, J. R. & Chu, S. (1999). Ligand-induced conformational changes observed in single RNA molecules. *Proc. Natl Acad. Sci. USA*, **96**, 9077–9082.
23. Kim, H. D., Nienhaus, G. U., Ha, T., Orr, J. W., Williamson, J. R. & Chu, S. (2002). Mg^{2+}-dependent conformational change of RNA studied by fluorescence correlation and FRET on immobilized single molecules. *Proc. Natl Acad. Sci. USA*, **99**, 4284–4289.
24. McKinney, S. A., Declais, A., Lilley, D. & Ha, T. (2003). Structural dynamics of individual Holliday junctions. *Nature Struct. Biol.* **10**, 93–97.
25. McKinney, S. A., Freeman, A. D., Lilley, D. M. & Ha, T. (2005). Observing spontaneous branch migration of Holliday junctions one step at a time. *Proc. Natl Acad. Sci. USA*, **102**, 5715–5720.
26. Lee, J. Y., Okumus, B., Kim, D. D. & Ha, T. (2005). Extreme conformational diversity in human telomeric DNA. *Proc. Natl Acad. Sci. USA*, **102**, 18938–18943.
27. Xie, Z., Srividya, N., Sosnick, T. R., Pan, T. & Scherer, N. F. (2004). Single-molecule studies highlight conformational heterogeneity in the early folding steps of a large ribozyme. *Proc. Natl Acad. Sci. USA*, **101**, 534–539.
28. Fang, X.-W., Golden, B. L., Littrell, K., Shelton, V., Thiyagarajan, P., Pan, T. & Sosnick, T. R. (2001). The thermodynamic origin of the stability of a thermophilic ribozyme. *Proc. Natl Acad. Sci. USA*, **98**, 4355–4360.
29. Fang, X.-W., Pan, T. & Sosnick, T. (1999). Mg^{2+}-dependent folding of a large ribozyme without kinetic traps. *Nauret Struct. Biol.* **6**, 1091–1095.
30. Fang, X.-W., Thiyagarajan, P., Sosnick, T. R. & Pan, T. (2002). The rate-limiting step in the folding of a large ribozyme without kinetic traps. *Proc. Natl Acad. Sci. USA*, **99**, 8518–8523.
31. Smith, G. J., Sosnick, T. R., Scherer, N. F. & Pan, T. (2005). Efficient fluorescence labeling of a large RNA through oligonucleotide hybridization. *RNA*, **11**, 234–239.
32. Kazantsev, A., Krivenko, A., Harrington, D., Holbrook, S., Adams, P. & Pace, N. (2005). Crystal structure of a bacterial ribonuclease P RNA. *Proc. Natl Acad. Sci. USA*, **102**, 13392–13397.
33. Qu, X., Smith, G. S., Lee, K. T., Sosnick, T. R., Pan, T. & Scherer, N. F. (2008). Single-molecule non-equilibrium periodic Mg^{2+}-concentration jump experiments reveal details of the early folding pathways of a large RNA. *Proc. Natl Acad. Sci. USA*, In press, doi:10.1073/PNAS.0801436105.
34. Colquhoun, D. & Hawkes, A. G. (1982). On the stochastic properties of bursts of single ion channel openings and of clusters of bursts. *Philos. Trans. R. Soc. Ser. B*, **300**, 1–59.
35. Buranachai, C., McKinney, S. A. & Ha, T. (2006). Single molecule nanometronome. *Nano Lett.* **102**, 18938–18943.
36. Yang, S. & Cao, J. (2001). Two-event echos in single-molecule kinetics: a signature of conformational fluctuations. *J. Phys. Chem. B*, **105**, 6536–6549.
37. Witkoskie, J. & Cao, J. (2004). Single molecule kinetics. I. Theoretical analysis of indicators. *J. Chem. Phys.* **121**, 6373–6379.
38. Selvin, P. (1995). Fluorescence Resonance Energy Transfer. *Methods Enzymol.* **246**, 300–334.
39. Callen, H. B. (1985). A Polymer Model: The Rubber Band Revisited. In *Thermodynamics; an Introduction to the Physical Theories of Equilibrium Thermostatics and Irreversible Thermodynamics*, 2nd edit., pp. 339–342. John Wiley and Sons, Inc., New York.
40. Murphy, M. C., Rasnik, I., Cheng, W., Lohman, T. M. & Ha, T. (2004). Probing Single-stranded DNA conformational flexibility using fluorescence spectroscopy. *Biophys. J.* **86**, 2530–2537.
41. Smith, S. B., Finzi, L. & Bustamante, C. (1992). Direct mechanical measurements of the elasticity of single DNA molecules by using magnetic beads. *Science*, **258**, 1122–1126.
42. Sosnick, T. R., Fang, X. W. & Shelton, V. M. (2000). Application of circular dichroism to study RNA folding transitions. *Methods Enzymol.* **317**, 393–409.
43. Pan, J., Thirumalai, D. & Woodson, S. A. (1999). Magnesium-dependent folding of self-splicing RNA: Exploring the link between cooperativity, thermodynamics, and kinetics. *Proc. Natl Acad. Sci. USA*, **96**, 6149–6154.
44. Thirumalai, D., Lee, N., Woodson, S. A. & Klimov, D. K. (2001). Early events in RNA folding. *Annu. Rev. Phys. Chem.* **52**, 751–762.
45. Bonnet, G., Krichevsky, O. & Libchaber, A. (1998). Kinetics of conformational fluctuations in DNA hairpin-loops. *Proc. Natl Acad. Sci. USA*, **95**, 8602–8606.
46. Krantz, B. A., Mayne, L., Rumbley, J., Englander, S. W. & Sosnick, T. R. (2002). Fast and slow intermediate accumulation and the initial barrier mechanism in protein folding. *J. Mol. Biol.* **324**, 359–371.
47. Dorywalska, M., Blanchard, S. C., Gonzalez, R. L., Jr, Kim, H. D., Chu, S. & Puglisi, J. D. (2005). Site-specific labeling of the ribosome for single-molecule spectroscopy. *Nucleic Acids Res.* **33**, 182–189.
48. Fang, X., Pan, T. & Sosnick, T. R. (1999). A thermodynamic framework and cooperativity in the tertiary folding of a Mg^{2+}-dependent ribozyme. *Biochemistry*, **38**, 16840–16846.
49. Rasnik, I., Myong, S., Cheng, W., Lohman, T. M. & Ha, T. (2004). DNA-binding orientation and domain conformation of the *E. coli* Rep helicase monomer bound to a partial duplex junction: single-molecule studies of fluorescently labeled enzymes. *J. Mol. Biol.* **336**, 395–408.
50. Graneli, A., Yeykal, C., Prasad, T. K. & Greene, E. C. (2006). Organized arrays of individual DNA molecules tethered to supported lipid bilayers. *Langmuir*, **22**, 292–299.
51. Ha, T. (2001). Single molecule fluorescence resonance transfer. *Methods*, **25**, 78–86.
52. Qu, X. W., Wu, D., Mets, L. & Scherer, N. F. (2004). Nanometer-localized multiple single-molecule fluorescence microscopy. *Proc. Natl Acad. Sci. USA*, **101**, 11298–11303.
53. Haran, G. (2004). Noise reduction in single-molecule fluorescence trajectories of folding proteins. *Chem. Phys.* **307**, 137–145.
54. Truhlar, D. & Garrett, B. (1980). Variational transition state theory. *Accts Chem. Res.* **13**, 440–448.